Results in Engineering 24 (2024) 103003

Contents lists available at ScienceDirect

Results in Engineering

journal homepage: www.sciencedirect.com/journal/results-in-engineering

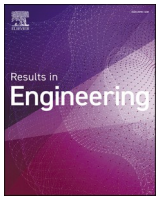

An ultra-compact microstrip bandpass filtering coupler with suppressed harmonics and low group delay: A novel structure for 5G applications

Salah I. Yahya [a,b], Farid Zubir [c,*], Leila Nouri [d,e,**], Noorlindawaty Md Jizat [f,***]

[a] Department of Communication and Computer Engineering, Cihan University-Erbil, Erbil, 44001, Iraq
[b] Department of Software Engineering, Faculty of Engineering, Koya University, Koya, KOY45, Iraq
[c] Wireless Communication Centre, Faculty of Electrical Engineering, Universiti Teknologi Malaysia, 81310, Johor Bahru, Johor, Malaysia
[d] Institute of Research and Development, Duy Tan University, Da Nang, 550000, Viet Nam
[e] School of Engineering & Technology, Duy Tan University, Da Nang, 550000, Viet Nam
[f] Faculty of Engineering, Multimedia University, Persiaran Multimedia, 63100, Cyberjaya, Selangor, Malaysia

ARTICLE INFO

Keywords:
Microstrip coupler
Compact
Group delay
Balanced magnitude
5G

ABSTRACT

This study introduces a novel microstrip design methodology for an ultra-compact bandpass filtering coupler, emphasizing a systematic approach to its development. The coupler is accurately designed, optimized, fabricated, and measured, achieving a small layout area of 0.003 λg^2, excluding feeding ports. The design process begins with a comprehensive mathematical analysis of a fundamental microstrip layout, followed by simultaneous optimization techniques that enhance performance characteristics. Electromagnetic simulations and measurements are conducted to validate the design, revealing an excellent correlation between the two and confirming precise performance metrics. The coupler demonstrates a filtering response with a suppressed 3rd harmonic and exhibits S_{21} and S_{31} values of −3.135 dB and −3.103 dB, respectively, indicating low insertion losses and balanced output magnitudes. Its isolation factor exceeds −19.5 dB across the frequency range from DC up to 1.875 GHz, making it particularly suitable for 5G applications. Additionally, the coupler features flat channels with minimal group delays, with S_{21} and S_{31} showing the maximum group delays close to 0.8 ns. Our design methodology not only integrates these advantages but also sets a new benchmark for compact bandpass filtering couplers, delivering exceptional performance within a remarkably constrained footprint.

1. Introduction

The low profile, light weight, and simplicity of fabrication of microstrip technology make it a widely favored design technique for RF and microwave devices such as antennas [1–4], filters [5–7], diplexers [8] and power dividers [9]. Recently, passive microstrip filtering devices have been widely used in modern wireless communications [5–13]. Among them, microstrip couplers are widely used in balanced mixers, power monitoring, power dividers, balanced amplifiers and combiners. For wireless communication systems, a coupler with filtering frequency response and suppressed harmonics is more attractive [14–16]. However, some microstrip couplers without filtering frequency responses are designed in Refs. [17–20]. A common disadvantage of the proposed microstrip couplers in Refs. [16–20] is occupying large implementation areas. Several types of microstrip structures are used for designing some couplers in Refs. [21–26]. To achieve a branch line coupler, a configuration similar to the conventional branch line but with long feeding lines is presented in Ref. [21]. Using this structure has caused an excessive increase in its size. Based on coupled lines, a novel microstrip filtering 0° coupler is designed in Ref. [22]. The problems of this coupler are its unbalanced magnitude and large size. The proposed microstrip branch-line coupler in Ref. [23] has unbalanced magnitude and phase. The structure of this coupler is such that the main body of the conventional structure is engraved and two T-shaped stubs are loaded inside it. The large size meandrous microstrip lines are utilized to obtain a filtering branch line coupler in Ref. [24]. Two-section microstrip-slot branch line coupler is introduced in Ref. [25]. This coupler has phase imbalance, large size and unsuppressed harmonics. Using a new

* Corresponding author.
** Corresponding author. Institute of Research and Development, Duy Tan University, Da Nang, 550000, Viet Nam.
*** Corresponding author.
E-mail addresses: faridzubir@utm.my (F. Zubir), leilanouri@duytan.edu.vn (L. Nouri), noorlindawaty.jizat@mmu.edu.my (N.M. Jizat).

https://doi.org/10.1016/j.rineng.2024.103003
Received 6 August 2024; Received in revised form 15 September 2024; Accepted 24 September 2024
Available online 25 September 2024

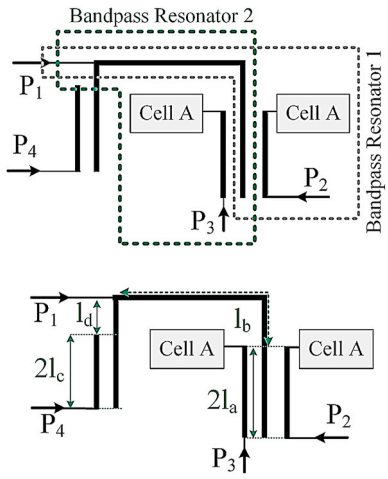

Fig. 1. Basic configuration of our coupler.

symmetrical structure, a triple-band microstrip coupler is designed in Ref. [26]. Considering that the need for telecommunication systems for devices that work in 5G frequencies has increased, the tendency to design in these frequencies has increased [27]. Designing a microstrip coupler that meets specific filtering requirements often involves complex geometries and precise dimensions, which can complicate the fabrication process [28]. Meanwhile, microstrip structures inherently have losses due to dielectric and conductor materials. These losses can degrade the filtering performance, especially at higher frequencies. On the other hand, attaining sharp frequency selectivity can be challenging. The filtering coupler proposed in Ref. [28], could not obtain an acceptable frequency selectivity. The bandwidth of a filter needs to be carefully designed, as too wide a bandwidth may not meet filtering requirements [29]. Another difficulty in designing a filtering coupler, is ensuring proper impedance matching across all ports. Mismatches can lead to reflections and reduced filtering effectiveness. Addressing these challenges typically requires a combination of careful design, advanced simulation techniques, and precise fabrication processes.

Our goal here is to achieve a filtering microstrip coupler with good frequency selectivity, small dimensions, low losses, balanced magnitude and low group delay. In this work, an innovative microstrip coupler for 5G mid-band applications is presented. This coupler has a new layout and good performance with suppressed harmonics from the 1st up to the 3rd. This coupler is miniaturized with a very compact size of 0.003 λg^2. The mathematical design technique is started by proposing an LC model of a new semi-layout structure. Then, the scattering parameters are calculated and analyzed for a predetermined operating frequency and a terminal impedance of 50Ω. After the designing process, it is simulated, fabricated and measured. Finally, it is compared with the other microstrip couplers to verify the advantages of this coupler. Despite the fact that most coupler designers have not considered group delay improvement, the proposed coupler can reduce this factor significantly. While microstrip filtering couplers have versatile applications, their scalability and effectiveness can be influenced by design complexity, manufacturing methods, and specific application requirements. Due to having filtering frequency response, this coupler is typically intended for use in communication systems for signal routing, splitting, and combining. Also, it can be employed in various signal processing applications where specific frequency bands need to be isolated or combined.

2. Analyzing the basic structure

Analyzing a microstrip basic structure can help in designing a microstrip filtering coupler by providing insights into the behavior and characteristics of microstrip transmission line. By understanding the electrical properties of the microstrip structure, designers can optimize coupler design to reach the desired performance. Accordingly, first a microstrip structure is proposed and analyzed.

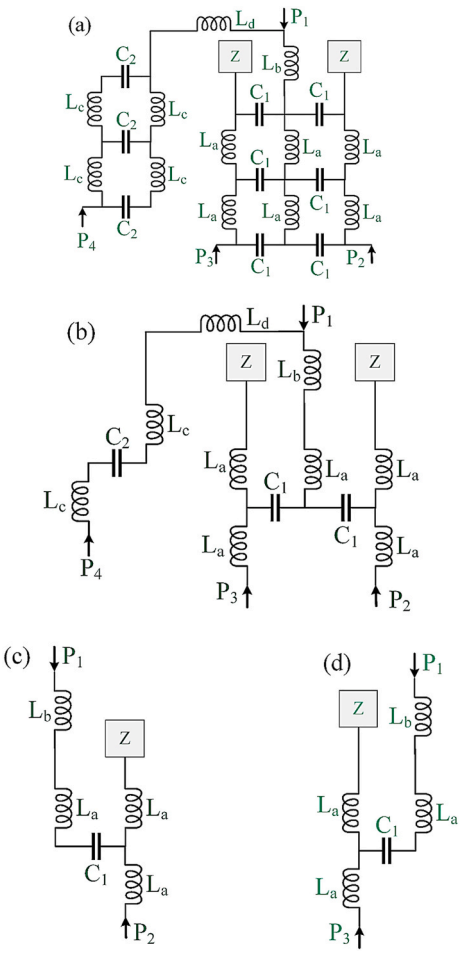

Fig. 2. (a): LC model of the presented coupler, (b) approximated LC model of the introduced coupler, (c) LC circuit of Bandpass Resonator 1, (d) LC circuit of Bandpass Resonator 2.

2.1. Introducing the proposed basic structure

To obtain a bandpass filtering coupler, we can use a 4-port microstrip structure consisting of coupled lines and additional stubs. Because, for creating the bandpass channels, coupled lines play an important role. By employing a symmetrical layout between Ports 2 (direct output port) and 3 (coupled output port), two channels can overlap significantly. Port 1 and Port 4 are the common input port and the isolation port, respectively. Accordingly, the semi-layout of the introduced coupler is presented in Fig. 1. It has two similar cells (named Cell A) connected to the coupled lines. The sections that help to create bandpass channels are marked as Bandpass Resonator 1 and Bandpass Resonator 2 in Fig. 1. An LC model (approximated) of the basic semi-layout is depicted in Fig. 2 (a). The coupling effects are depicted by capacitors C_1 and C_2. The inductors L_a and L_c are the equivalents of the transition lines l_a and l_c respectively. Also, l_b and l_c are replaced by the inductor L_b and the inductor L_c. In this approximated LC circuit, the bents effects are ignored. Since, the bents have very weak effects at the frequencies lower than 10 GHz.

Due to the complex LC circuit, more approximations are applied for easy calculations. Fig. 2(b) depicts the approximated LC circuit, where the coupling effects are presented by only three capacitors. The equivalents of Bandpass Resonator 1 and Bandpass Resonator 2 are depicted

in Fig. 2(c) and (d).

2.2. Analyzing the bandpass resonators

Based on the equivalent circuits displayed in Fig. 2(c) and (d), the transfer matrices of Bandpass Resonator 1 and Bandpass Resonator 2 (M_{T1} and M_{T2}) can be given by:

$$M_T = M_{T1} = M_{T2} = \begin{bmatrix} 1 & j\omega(L_a+L_b)+\frac{1}{j\omega C_1} \\ 0 & 1 \end{bmatrix} \times \begin{bmatrix} 1 & 0 \\ \frac{1}{Z+j\omega L_a} & 1 \end{bmatrix} \times \begin{bmatrix} 1 & j\omega L_a \\ 0 & 1 \end{bmatrix} \quad (1)$$

Z is the impedance of the microstrip Cell A. According to the symmetrical structure, the transfer matrices of Bandpass Resonator 1 and Bandpass Resonator 2 are the same. After calculation, Equation (1) can be simplified as follows:

$$M_T = \begin{bmatrix} 1+\frac{j\omega(L_a+L_b)+\frac{1}{j\omega C_1}}{Z+j\omega L_a} & \frac{L_a}{C_1}-\omega^2 L_a(L_a+L_b) \\ \frac{1}{Z+j\omega L_a} & 1+\frac{j\omega L_a}{Z+j\omega L_a} \end{bmatrix} \frac{}{Z+j\omega L_a}+j\omega(2L_a+L_b)+\frac{1}{j\omega C_1} \quad (2)$$

C_1 is usually in pF or fF. Our aim is to have an operating frequency in GHz, while the inductors L_a and L_b are in nH. So, we can apply some approximations as written in Equation (3.c), (3.b) and (3.a):

$$j\omega(L_a+L_b)+\frac{1}{j\omega C_1} \approx \frac{1}{j\omega C_1} \quad (3.a)$$

$$\frac{L_a}{C_1}-\omega^2 L_a(L_a+L_b) \approx \frac{L_a}{C_1} \quad (3.b)$$

$$j\omega(2L_a+L_b)+\frac{1}{j\omega C_1} \approx \frac{1}{j\omega C_1} \quad (3.c)$$

Substituting Equation (3.c), (3.b) and (3.a) in Equation (2) leads to:

$$M_T \approx \begin{bmatrix} 1+\frac{j\omega(L_a+L_b)}{Z+j\omega L_a} & \frac{1}{C_1}\left(\frac{L_a}{Z+j\omega L_a}+\frac{1}{j\omega}\right) \\ \frac{1}{Z+j\omega L_a} & \frac{j\omega L_a}{j\omega L_a+Z}+1 \end{bmatrix} \quad (4)$$

Using Equation (4), the scattering parameters can be extracted for the 50Ω terminals as follows [30]:

$$S_{21}=S_{31}=\frac{2}{2+\frac{j\omega(2L_a+L_b)}{Z+j\omega L_a}+\frac{1}{50C_1}\left(\frac{L_a}{j\omega L_a+Z}+\frac{1}{j\omega}\right)+\frac{50}{j\omega L_a+Z}} \quad (5)$$

Due to having a very small coupling capacitor, similar to Equation (3.c), (3.b) and (3.a), it can be written:

$$\frac{1}{50C_1}\left(\frac{L_a}{Z+j\omega L_a}+\frac{1}{j\omega}\right) \gg 2+\frac{j\omega(2L_a+L_b)}{Z+j\omega L_a}+\frac{50}{Z+j\omega L_a} \quad (6)$$

Therefore, S_{21} and S_{31} can be obtained as follows:

$$S_{21}=S_{31} \approx \frac{100j\omega(Z+j\omega L_a)C_1}{2j\omega L_a+Z} \quad (7)$$

Based on the above approximations, L_b is removed in Equation (7). Equation (7) determines the behavior of the proposed resonator. For reducing the losses at the operating frequency of each resonator, it is better to set $|S_{21}| = |S_{31}| = 1$. If we set the operating frequency at 1.1 GHz, using $|S_{21}| = |S_{31}| = 1$, it can be written that:

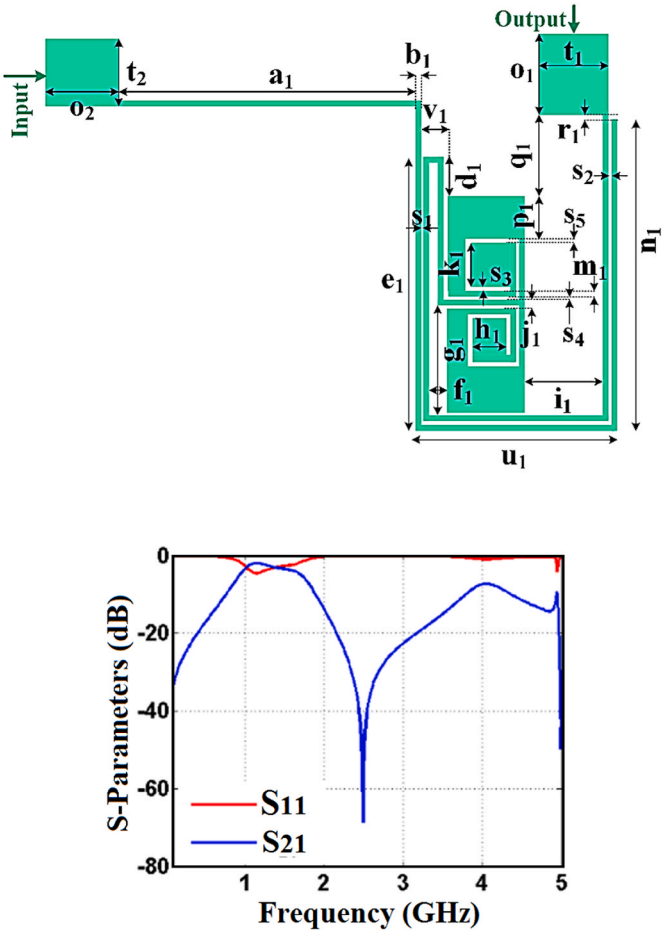

Fig. 3. Bandpass Resonator 1: layout and frequency response.

$$j\frac{220\pi(Z+2.2j\,L_a)C_1}{4.4jL_a+Z} \approx 1 \rightarrow Z \approx \frac{-4.4j+484\pi\,C_1}{220\pi C_1 j+1}L_a \quad (8)$$

Thus, according to Equation (8) the impedance Z can be calculated. For small coupling capacitors, this value depends on L_a, so under this condition $Z \sim -j4.4L_a$ Ω at $\omega_o = 2.2\pi$ GHz, where ω_o is the angular operating frequency. Hence, Z is a capacitor and the microstrip Cell A is a section with the capacitance feature. Decreasing L_a leads to an increase in this capacitor. Therefore, this capacitor can be increased as much possible as to decrease the overall size. However, Cell A can be so large that we do not need to increase the size. By tuning the area of Cell A, the physical length l_a and the space of coupled lines, the impedance Z, the inductance L_a and the capacitor C_1 can be controlled. Therefore, according to Equation (8) a method to reduce losses is adjusting the physical length l_a, the area of Cell A and the gap between coupled lines. Also, by tuning these parameters the resonance frequency can be tuned. Meanwhile, the overall size can be miniaturized based on Equation (8). For this purpose, the length l_a and Z can be reduced. Under this condition the overall size will be decreased, where the operating frequency is fixed. For decreasing Z, the dimension of Cell A should be increased. Since Cell A is an internal stub, it cannot increase the overall size. These results are verified by the simulation data.

2.3. Analyzing the isolation section

To analyze the isolation section, the impedance between ports 1 and 4 ($Z_{1,4}$) is calculated as follows:

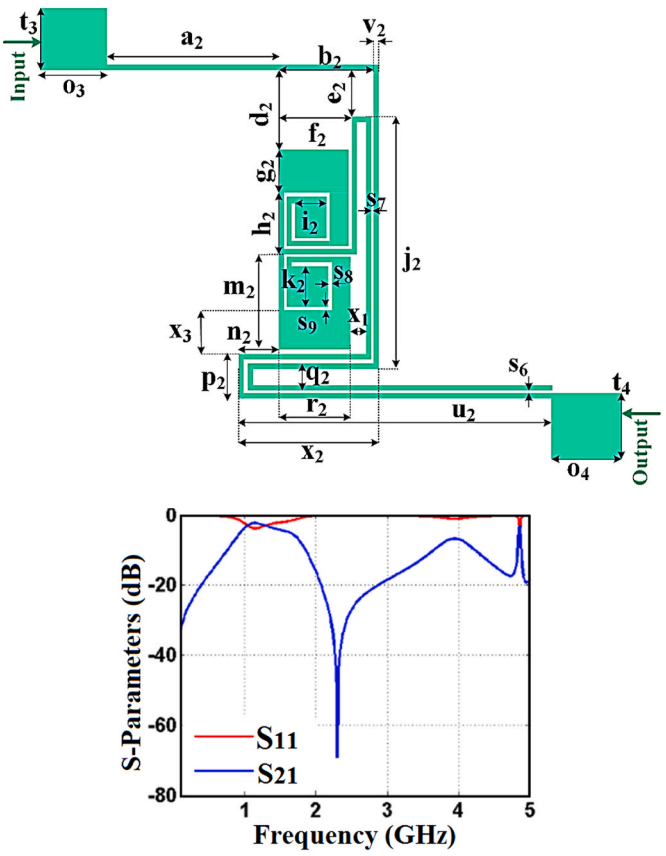

Fig. 4. Bandpass Resonator 2: layout and frequency response.

$$Z_{1,4} = j\omega(2L_c + L_d) + \frac{1}{j\omega C_2} \tag{9}$$

C_2 is usually in pF or fF, while the inductors L_c and L_d are in nH. Accordingly:

$$j\omega(2L_c + L_d) \langle\langle \frac{1}{j\omega C_2} \tag{10}$$

Applying Equation (10) in Equation (9) leads to:

$$Z_{1,4} \approx \frac{1}{j\omega C_2} \tag{11}$$

Therefore, the transfer matrix between the common and isolation ports (M_I) can be derived as follows:

$$M_I = \begin{bmatrix} 1 & \frac{1}{j\omega C_2} \\ 0 & 1 \end{bmatrix} \tag{12}$$

Table 2
Performance of the proposed bandpass resonators (BPR_1 and BPR_2 are Bandpass Resonators 1 and 2 respectively).

Design	F_r	IL	FBW	Harmonic Level	N^{th} Suppressed Harmonic	Last Frequency with Suppressed Harmonics
BPR_1	1.1 GHz	−2.063 dB	31 %	−15 dB	2^{nd}	3.5 GHz
BPR_2	1.1 GHz	−2.3 dB	21.5 %	−15 dB	2^{nd}	3.3 GHz

Using Equation (12), S_{41} is extracted for the 50Ω terminals as follows:

$$S_{41} = \frac{100j\omega C_2}{100j\omega C_2 + 1} \tag{13}$$

since $100j\omega C_2 << 1$, it can be said that $S_{41} \sim 100j\omega C_2$, which verifies having small S_{41} at the passband. Therefore, the isolation port works correctly and this section can be added to the three-port microstrip cell.

3. Designing bandpass resonators using the analyzed basic structure

Using the analyzed basic structures of Bandpass Resonator 1 and Bandpass Resonator 2, two resonators are designed. Figs. 3 and 4 show the frequency responses and layouts of these resonators. The feeding sections connected to the output/input ports are wisely chosen to be near 50 Ω on an RT/Duroid 5880 substrate. RT/Duroid 5880 with a dielectric constant of 2.2 is an excellent choice for a microwave application due to its low loss, stable properties and ease of fabrication. This substrate has a low loss tangent, which results in minimal signal attenuation. This is crucial for high-frequency applications where signal integrity is paramount. The dielectric constant of 2.2 is stable across a wide frequency range, ensuring consistent performance in various operating conditions. Moreover, RT/Duroid 5880 offers good mechanical strength and durability, which helps maintain the integrity of the circuit during fabrication and operation. Also, the lightweight nature of the substrate makes it advantageous for applications where weight is a critical factor, such as in aerospace. As shown in Figs. 3 and 4, both resonators can operate near 1.1 GHz. All simulation results in this paper are extracted from Advanced Design System software. The dimensions of Bandpass resonators are shown in Table 1. Table 2 shows the performance of the proposed bandpass resonators. In this Table, F_r, FBW and IL are the resonance frequency, fractional bandwidth and insertion loss respectively.

4. Obtaining the proposed filtering coupler

The proposed resonators are integrated to achieve a 0° filtering

Table 1
Physical dimensions of the proposed bandpass resonators.

Parameters	Size (mm)	Parameters	Size (mm)	Parameters	Size (mm)	Parameters	Size (mm)	Parameters	Size (mm)
a_1	9	g_2	1.4	n_1	1.3	r_2	2.3	t_2	2
a_2	5.9	h_1	1.3	n_2	1.4	s_1	0.1	t_3	2
b_1	0.1	h_2	2	o_1	2.2	s_2	0.1	t_4	2.1
b_2	3.1	i_1	2.5	o_2	2.2	s_3	0.1	u_1	5.4
d_1	1.1	i_2	1.1	o_3	2.2	s_4	0.1	u_2	10.5
d_2	2.6	j_1	0.2	o_4	2.2	s_5	0.1	v_1	0.9
e_1	8.2	j_2	8.2	p_1	1.4	s_6	0.1	v_2	0.1
e_2	1.5	k_1	1.4	p_2	1.3	s_7	0.1	x_1	0.6
f_1	0.6	k_2	1.4	q_1	2.5	s_8	0.1	x_2	4.6
f_2	2.4	m_1	0.1	q_2	0.9	s_9	0.1		
g_1	3.4	m_2	3.3	r_1	0.1	t_1	2.1		

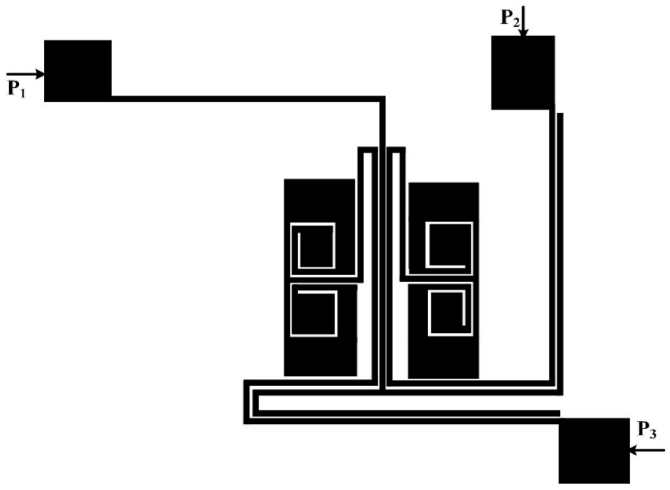

(a)

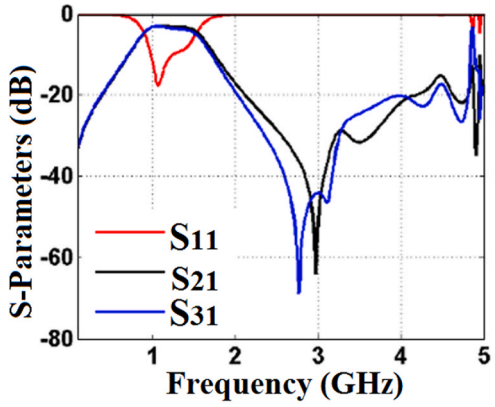

(b)

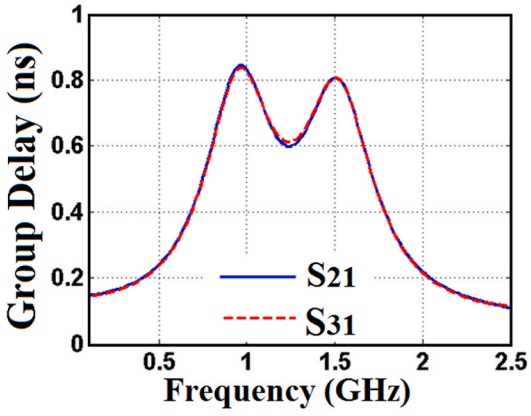

(c)

Fig. 5. (a) A three-port microstrip cell composed of the proposed bandpass resonators, (b) frequency response of the three-port microstrip cell, (c) group delay of the three-port microstrip cell.

coupler. After connecting the microstrip resonators, there is a three-port microstrip cell as illustrated in Fig. 5(a). This cell has two similar cells placed inside the empty space. The dimensions of three-port microstrip cell are exactly equal to the proposed bandpass resonators. The frequency response and group delay of this three-port microstrip cell are depicted in Fig. 5(b) and (c). As presented in Fig. 5(b), integrating these resonators has a positive loading effect. Because, the harmonics are

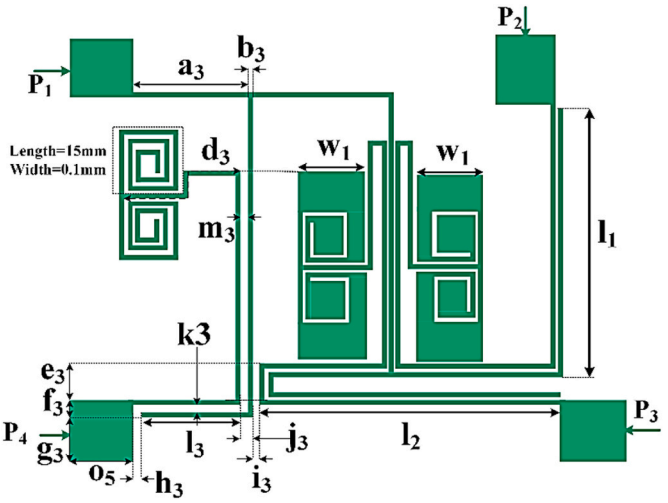

Fig. 6. Layout configuration of the presented coupler.

suppressed and return loss is improved. As presented in Fig. 5(c), S_{21} and S_{31} have the group delays better than 1ns inside the passbands.

The proposed coupler including the isolation section, Bandpass Resonator 1 and Bandpass Resonator 2 is shown in Fig. 6. The size of our presented coupler including all ports is 19.4 mm × 14.8 mm (0.006 λg^2). Without the 50 Ω feeding lines, the coupler size is 15.3 mm × 11.3 mm (0.003 λg^2). The spiral cells, which are electrically connected to Port 4 are added to improve the isolation. The dimensions of the proposed coupler are exactly equal to the presented three-port cell. After adding Port 4 (P4), it was necessary to show some dimensions as depicted in Table 3. Reducing the size of this microstrip coupler is achieved through several techniques, primarily focusing on the use of innovative resonator designs. Employing techniques such as meandered geometries effectively increases the electrical length of the resonator without significantly increasing its physical footprint. By increasing the size of internal patch cells, the operating bandwidth moves to the left without increasing the overall physical size. On the other hand, incorporating coupled resonators could further minimize the size by allowing for compact integration of multiple resonant elements. Finally, optimization helps to reduce the overall size of the proposed coupler again. These strategies collectively contribute to the miniaturization of our microstrip coupler while preserving its functionality and performance characteristics.

5. Optimization

A part of the optimization steps is shown in Fig. 7 (a)-Fig. 7(f). In these figures, the frequency responses are depicted as some functions of the physical dimensions l_1, l_2, l_3 and w_1. Fig. 7(a) and (b) confirm that some harmonics appear by increasing l_1 and l_2. Therefore, we cannot increase l_1 and l_2 too much. However, decreasing these physical lengths can shift the operating frequency to the higher frequencies. This increases the overall size in λg^2. Therefore, the lengths of these coupled lines should be carefully chosen. If the distance between the coupled lines is minimized, the probability of manufacturing errors increases significantly. Additionally, selecting a width for these transmission lines that is less than 0.1 mm greatly heightens the risk of inaccuracies during fabrication. These factors impose critical constraints on the design to ensure reliable manufacturing outcomes. As shown in Fig. 7(c), decreasing l_3 can improve the isolation factor. By decreasing w_1 the return loss is improved (see Fig. 7(d)). In addition, some harmonics appear when increasing w_1 (Fig. 7(e) and (f)). Based on Equation (7), by increasing the length of coupled lines (l_a), the resonant frequency shifts to the left when other parameters are constant. This is verified by the simulation results presented in Fig. 7(a) and (b). If the length of the

Table 3
Physical dimensions of the proposed coupler after adding P4.

Parameters	Size (mm)	Parameters	Size (mm)	Parameters	Size (mm)	Parameters	Size (mm)
a_3	4.1	f_3	0.6	j_3	0.5	l_3	3.5
b_3	0.1	g_3	1.5	k_3	0.4	m_3	0.4
d_3	4.7	h_3	0.2	l_1	9.5	o_5	2.2
e_3	1.2	i_3	0.3	l_2	10.5		

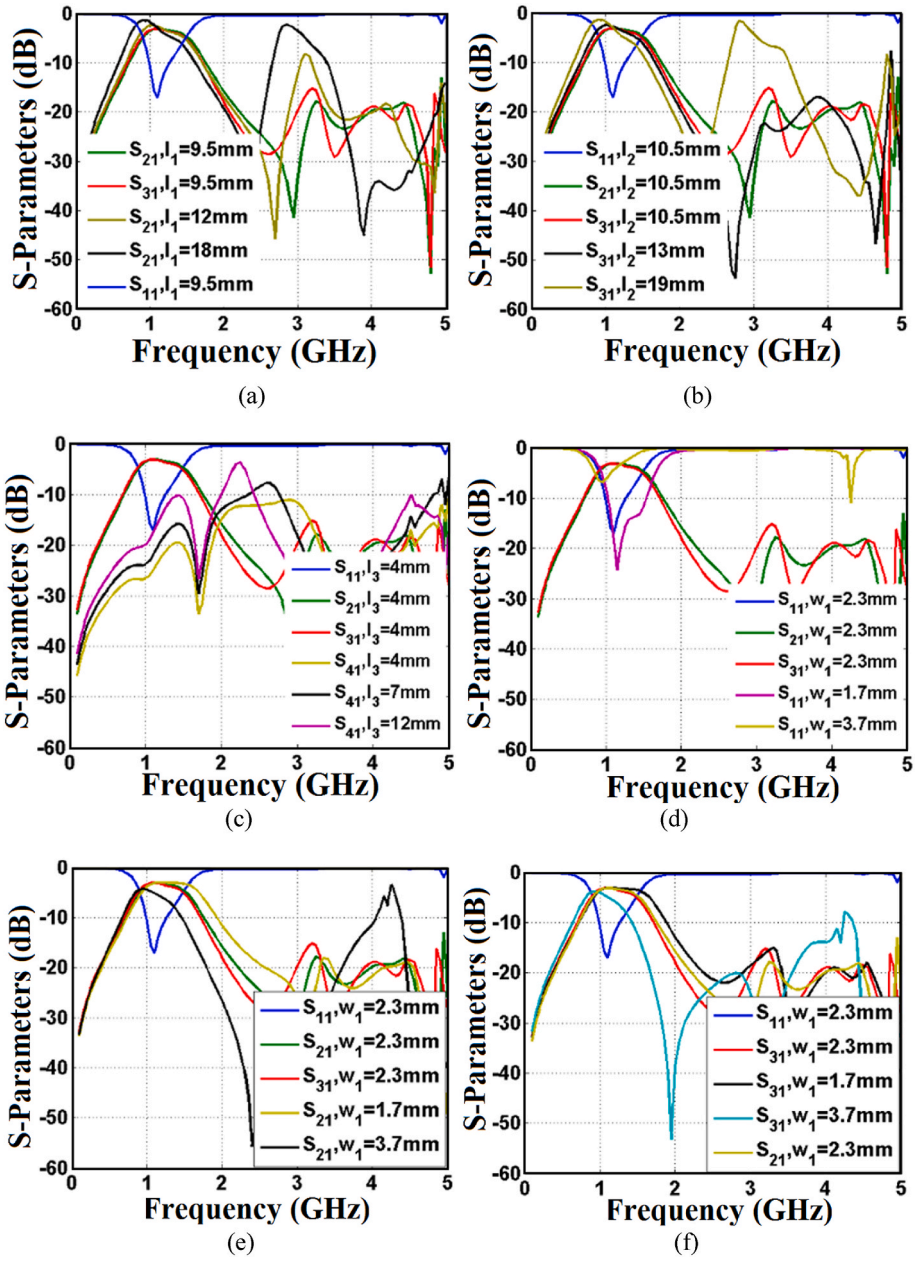

Fig. 7. A summary of the optimization; frequency responses as functions of the physical lengths (a) l_1, (b) l_2, (c) l_3, (d) the effect of changing w_1 on S_{11}, (e) the effect of changing w_1 on S_{21}, (f) the effect of changing w_1 on S_{31}.

coupled lines l_c increases, the capacitor created by them (C_2) increases. Based on Equation (13) $S_{41}\approx j\omega C_2$ (because $100j\omega C_2<<1$). So, by increasing C_2 the value of S_{41}(dB) increases. This is confirmed in Fig. 7 (c). As can be seen, S_{41} increases when increasing the length of the coupled lines connected to Port 4 (l_3).

Equations (13) and (7) can be used to determine the capacitors and inductors in the equivalent circuit model. This will involve calculating the equivalent inductance and capacitance based on the properties and dimensions of the microstrip resonator. Once the values of inductors and capacitors are achieved, the equivalent circuit model and its S-parameters will be achieved. This can be done using standard techniques for analyzing passive networks, such as the scattering matrix method. By following these steps, the equations can be used to find the behavior of a microstrip resonator by modeling it with an LC equivalent circuit and calculating its S-parameters. This approach provides a simplified representation of the complex microstrip structure and allows for easier

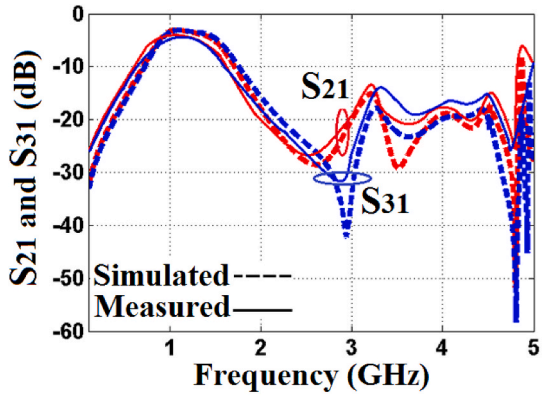

(a)

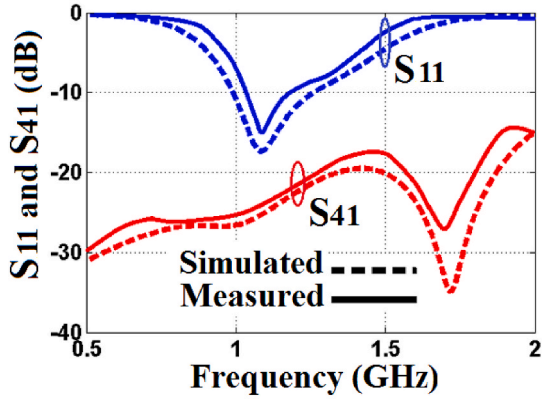

(b)

Fig. 8. S-parameters of the introduced coupler, (a) S_{31} and S_{21} (b) return loss (S_{11}) and isolation factor (S_{41}).

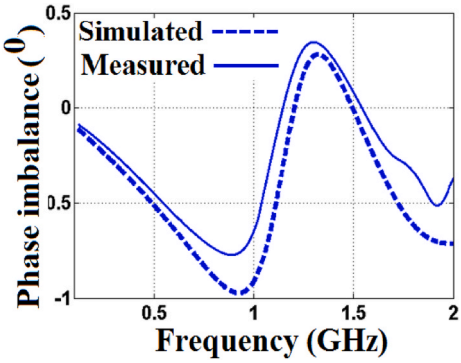

Fig. 9. Phase difference of S_{21} and S_{31}.

analysis and design optimization.

6. Results, comparison and discussion

As mentioned before, ADS software is used for the simulation. Also, HP8757A network analyzer is used for the measurement. In Fig. 8, the simulated and experimental scattering parameters of the introduced coupler are depicted. As can be seen, this coupler has a strong filtering response. It operates at 1.085 GHz, where S_{21} and S_{31} are −3.135 dB and −3.103 dB respectively. Therefore, the suggested coupler has low insertion losses and balanced magnitudes. This coupler works at 1.085 GHz. Maintaining quality control during scaling is critical, especially for high-frequency (higher than 10 GHz) applications where performance can be sensitive to manufacturing tolerances.

The maximum harmonic levels above the passbands up to 4.85 GHz are better than −15.1 dB. Also, the obtained isolation is below −19.5 dB for the frequencies less than 1.875 GHz, while at the operating frequency it is −25.3 dB. Meanwhile, at the operating frequency, S_{11} is −17.36 dB. The measured and simulated phase differences of S_{31} and S_{21} are displayed in Fig. 9. As can be seen, the phase imbalance at the operating frequency is 0.6°. To verify the superiority of this coupler, it is compared with some previous designs in Table 4. The fair parameters are chosen for comparison. It is clear that the most compact size, the most balanced magnitude, and the best harmonic suppression are achieved in this study simultaneously. Only, the suggested couplers in Refs. [14,20] could improve the phase balance better than this work. However, this coupler is more compact with better harmonic suppression.

In passive devices, group delay is one of the significant features in determining performance. However, most coupler designers have not paid attention to this subject. As shown in Fig. 10, the designed coupler has the maximum group delays of 0.829 ns and 0.826 ns for S_{21} and S_{31}. Since group delay is not reported in the previous couplers, in Table 5 the comparison is done with the other microstrip devices. It can be seen that the presented coupler has the lowest group delay. Since the channels are flat and wide, the group delays of S_{31} and S_{21} are reduced. As depicted in Fig. 7 (a), (b), (e) and (f) by tuning the width w_1 and the lengths l_1 and l_2, the flatness and bandwidth can be improved simultaneously. Fig. 11 shows the fabricated coupler.

Having low group delay and subsequently low distortion indicates good power tolerance of this coupler. On the other hand, the manufacturing error of this work is low and the measurement results and the simulation data are close to each other. According to the comparison table, the amount of losses is very low. These ensure that the proposed coupler meets the requirements for power handling capabilities. Therefore, it can be used in 5G applications. A summary of the obtained results for the proposed coupler is presented in Table 6.

The future of designing microstrip filtering couplers is poised for significant advancements driven by the increasing demand for compact, high-performance RF and microwave components in emerging technologies such as 5G, Internet of Things (IoT), and satellite communications. Innovations in materials, such as low-loss dielectrics and flexible substrates, will enhance the efficiency and miniaturization of couplers. Additionally, the integration of advanced simulation tools and artificial intelligence will enable designers to optimize performance parameters like bandwidth, selectivity, and power handling more effectively. Furthermore, the incorporation of metamaterials and novel geometries may lead to the development of multifunctional couplers that can operate across multiple frequency bands, thus catering to the diverse needs of modern communication systems. As a result, the future landscape will likely feature highly integrated, versatile, and cost-effective microstrip filtering couplers that meet the stringent requirements of next-generation applications.

7. Conclusion

A novel microstrip layout is proposed and mathematically analyzed to obtain a balanced 0° coupler. The microstrip cells connected to the direct and coupling output ports were similar, which helped to overlap the outputs. It has several advantages in terms of flat channels, compact size, suppressed harmonics, balanced magnitude, low insertion loss, filtering frequency response and low group delay. Having these advantages at the same time is a sign of the superiority of this coupler over the previous designs. Compared with the other microstrip passive devices, the maximum group delay of this coupler is very low. It operates at 1.085 GHz, which is appropriate for 5G mid-band applications. Also, the proposed approach in this paper offered a highly effective and efficient method for determining the S-parameters of microstrip resonators. By utilizing an LC equivalent model, this technique provided a simplified yet accurate representation of the complex microstrip structure. This

Table 4
Comparison with the previous designs.

Refs.	F_O (GHz)	S_{21}, S_{31} (dB)	S_{41} (dB)	Phase Imbalance	Magnitude Imbalance (dB)	FR	N^{th} SH	Size ($\lambda g^2/mm^2$)
This Work	1.085	−3.13, −3.1	−25.3	0.6°	0.032	Yes	3rd	0.003/172.9
[14]	5.2	−3.28, −3.56	−28.2	0.1°	0.28	Yes	2nd	0.04/83.2
[15]	–	−3.6, −3,6 ± 0.5	−20	–	0.5	Yes	No	0.23[b]/1157
[16]	2	−3.11, −3.39	–	1°	0.28	Yes	2nd	—/265
[17]	2	−3.1, −3.46	−20	3°	0.36	No	No	—/1322
[18]	3	−7.38, −2.25	−21.5	2.3°	5.13	No	No	—/819
[19]	0.433	−4.07, −4.39	−27.4	2.1°	0.32	No	No	—/2218
[20]	6	−3.9, −3.9	−18.9	0.5°	–	No	No	0.222/75.8
[22]	2.82	−3.3, −2.8	−31.3	0.97°	0.5	Yes	1st	0.075/710
[23]	3.5	−3.65, −2.97	−29.2	3.6°	0.68	No	No	0.0432/448
[24]	1.87	−4.4, −4.4 ± 0.5	−15[c]	3°	0.5	Yes	No	0.1386/—
[25] [a]	2.17,3.6, 5.9	–	–	5°	–	Yes	No	0.448/—

[a] Tri-channel.
[b] Approx.; SH: Suppressed harmonic; Fo: Operating frequency; FR: Filtering response.
[c] Better than −15 dB at all Passband.

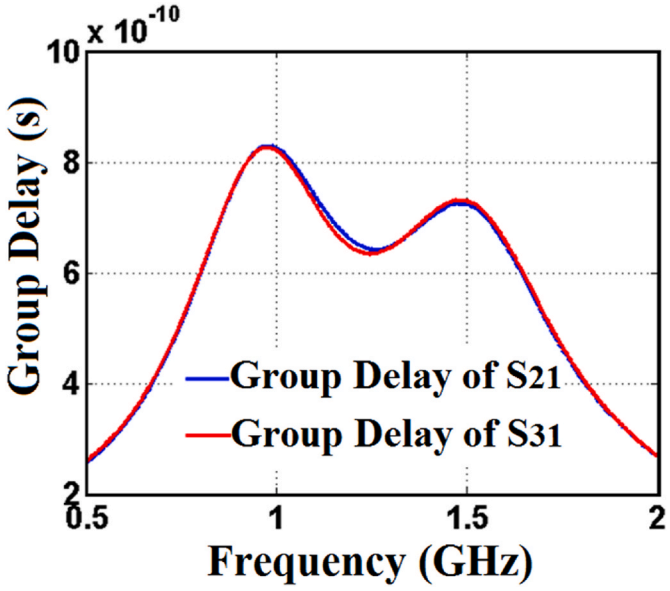

Fig. 10. Simulated group delays of S_{31} and S_{21}.

Table 5
Group delay comparison (BP-BP: Bandpass-Bandpass; BPF: Bandpass filter; LP-BP: Lowpass-Bandpass).

Refs.	Type	Maximum Group delay at all channels
This	Coupler	0.82 ns
[31]	LP-BP Triplexer	2.07 ns
[32]	LP-BP Diplexer	More than 2.5 ns
[33]	Tri-Channel BPF	8 ns
[34]	LP-BP Triplexer	6 ns
[35]	Quad-Channel BPF	9 ns
[36]	BP-BP Diplexer	Near 4 ns
[37]	BP-BP Diplexer	1.5 ns
[38]	Lowpass Filter	5.9 ns
[39]	Dispersive Filter	4.5 ns

approach offered significant advantages over traditional methods, including increased design flexibility, improved analysis capabilities, and reduced computational complexity. Additionally, the use of lumped elements allows for straightforward parameter extraction, enabling designers to quickly optimize their designs for maximum performance.

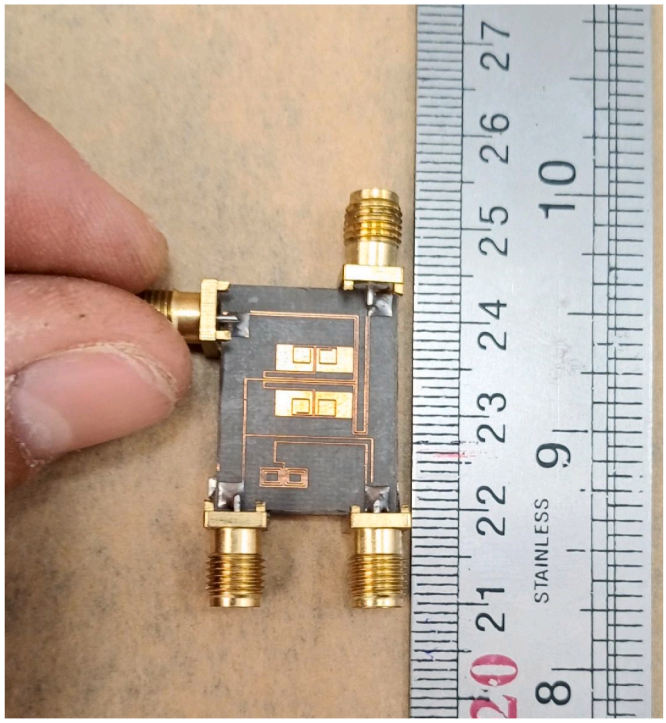

Fig. 11. Fabricated coupler.

Table 6
The obtained results for the proposed coupler.

Operating Frequency	1.085 GHz	Maximum Group delay of S_{21}	0.829 ns
S_{11} at the operating frequency	−17.36 dB	Maximum Group delay of S_{31}	0.826 ns
S_{21} at the operating frequency	−3.135 dB	Phase of S_{21} at the operating frequency	−64.791°
S_{31} at the operating frequency	−3.103 dB	Phase of S_{31} at the operating frequency	−64.156°
S_{41} at the operating frequency	−25.3 dB	Highest frequency with suppressed harmonic	4.85 GHz
Overall size	15.3 mm × 11.3 mm	Maximum harmonic level	−15.1 dB

CRediT authorship contribution statement

Salah I. Yahya: Writing – review & editing, Visualization, Validation, Resources, Methodology, Formal analysis. **Farid Zubir:** Writing – review & editing, Writing – original draft, Visualization, Validation, Supervision, Software, Resources, Project administration, Methodology, Investigation, Funding acquisition, Formal analysis, Data curation, Conceptualization. **Leila Nouri:** Writing – original draft, Validation, Software, Methodology, Investigation, Formal analysis, Data curation, Conceptualization. **Noorlindawaty Md Jizat:** Writing – review & editing, Writing – original draft, Visualization, Software, Resources, Project administration, Funding acquisition, Formal analysis, Conceptualization.

Declaration of competing interest

The authors declare that they have no known competing financial interests or personal relationships that could have appeared to influence the work reported in this paper.

Data availability

Data will be made available on request.

Acknowledgment

This work was supported in part by the Higher Institution Centre of Excellence (HICOE), Ministry of Higher Education Malaysia through the Wireless Communication Centre (WCC), Universiti Teknologi Malaysia (UTM) under Grant R.J090301.7823.4J610; in part by the UTM Fundamental Research (UTMFR) under Grant Q.J130000.3823.23H92; and in-part by the Faculty of Engineering, Multimedia University, Cyberjaya, Selangor, Malaysia.

References

[1] A. Youssef, I. Halkhams, R.E. Alami, M.O. Jamil, H. Qjidaa, A simulation study of dual band THz soft antenna for biomedical applications, Scientific African 25 (2024) e02294, https://doi.org/10.1016/j.sciaf.2024.e02294.
[2] S.E. Didi, I. Halkhams, A. Es-saqy, M. Fattah, S. Mazer, M.E. Bekkali, Creation of a soft circular patch antenna for bio-medical applications for 5G at frequency 2.45 GHz, Results in Engineering 22 (2024) 102319, https://doi.org/10.1016/j.rineng.2024.102319.
[3] A. Youssef, I. Halkhams, R.E. Alami, M.O. Jamil, H. Qjidaa, A new approach to designing a multiband antenna using photonic crystals and load graphene for terahertz application, Results in Engineering 22 (2024) 102327, https://doi.org/10.1016/j.rineng.2024.102327.
[4] A. Youssef, I. Halkhams, R.E. Alami, M.O. Jamil, H. Qjidaa, A novel slotted antenna design for future Terahertz applications, Int. J. Electr. Comput. Eng. 14 (3) (2024) 2708–2716, https://doi.org/10.11591/ijece.v14i3.pp2708-2716.
[5] Y. Khardioui, A.E. Alami, M.E. Ghzaoui, Design and optimization of a compact microstrip BPF for wireless communication systems based on open-loop rectangular resonators, Results in Engineering 21 (2024) 101941.
[6] M.R.A. Nasser, R.K. Jaiswal, D. Psychogiou, A compact bandpass filter manifold with ultra wide frequency and bandwidth tuning, in: IEEE Access, vol. 11, 2023, pp. 41054–41060, https://doi.org/10.1109/ACCESS.2023.3269884.
[7] Y. Khardioui, A.E. Alami, M.E. Ghzaoui, Design and optimization of a compact microstrip BPF for wireless communication systems based on open-loop rectangular resonators, Results in Engineering 21 (2024) 101941, https://doi.org/10.1016/j.rineng.2024.101941.
[8] L. Nouri, S.I. Yahya, A. Rezaei, F.A. Hazzazi, B.N. Nhu, A compact negative group delay microstrip diplexer with low losses for 5G applications: design and analysis, ARO-THE SCIENTIFIC JOURNAL OF KOYA UNIVERSITY 11 (2) (2023) 17–24.
[9] S. Roshani, I. Yahya Salah, Y.Y. Ghadi, S. Roshani, F. Parandin, B.D. Yaghouti, Size reduction and harmonics suppression in microwave power dividers: a comprehensive review, ARO-THE SCIENTIFIC JOURNAL OF KOYA UNIVERSITY 11 (2) (2023) 122–136.
[10] Z. Chao, Z. Zitong, X. Pei, A miniaturized microstrip antenna with tunable double band-notched characteristics for UWB applications, Sci. Rep. 12 (2022) 19703, https://doi.org/10.1038/s41598-022-24384-2.
[11] D. Li, C. Yang, Y. Liu, L. Zhang, Q. Chen, Integration design of passive filtering nonmagnetic circulator based on spatiotemporal modulation of microstrip filtering delay networks, IEEE Trans. Microw. Theor. Tech. (2023) 1–9, https://doi.org/10.1109/TMTT.2023.3311918.
[12] J. Gong, Y. Chen, B. Chen, J. Zhao, K. Xu, Z. Zhong, M. Liu, A compact microstrip second-order lossy bandpass filter with improved simplified composite right-/left-handed zeroth-order resonator, Microw. Opt. Technol. Lett. 66 (1) (2024), https://doi.org/10.1002/mop.34015.
[13] J. Xu, Z.Y. Chen, H. Wan, Lowpass-bandpass triplexer integrated switch design using common lumped-element triple-resonance resonator technique, IEEE Trans. Ind. Electron. 67 (1) (2020) 471–479.
[14] S.I. Yahya, F. Zubir, L. Nouri, F. Hazzazi, Z. Yusoff, M.A. Chaudhary, M. Assaad, A. Rezaei, B.N. Le, A balanced symmetrical branch-line microstrip coupler for 5G applications, Symmetry 15 (8) (2023) 1598, https://doi.org/10.3390/sym15081598.
[15] W.A. Arriola, J.Y. Lee, I.S. Kim, Wideband 3 dB branch line coupler based on λ/4 open circuited coupled lines, IEEE Microw. Wireless Compon. Lett. 21 (9) (2011) 486–488, https://doi.org/10.1109/LMWC.2011.2138687.
[16] J. Wang, B. Wang, Y. Guo, L. Ong, S. Xiao, A compact slow-wave microstrip branch-line coupler with high performance, IEEE Microw. Wireless Compon. Lett. 17 (7) (2007) 501–503, https://doi.org/10.1109/LMWC.2007.899307.
[17] Y. Chun, J. Hong, Compact wide-band branch-line hybrids, IEEE Trans. Microw. Theor. Tech. 54 (2) (2006) 704–709, https://doi.org/10.1109/TMTT.2005.862657.
[18] A.B. Santiko, Y.P. Saputera, Y. Wahyu, Design and implementation of three branch line coupler at 3.0 GHz frequency for S-band radar system, in: The 22nd Asia-Pacific Conference on Communications, 2016, pp. 315–318, https://doi.org/10.1109/APCC.2016.7581487.
[19] S. Velan, M. Kanagasabai, Compact microstrip branch-line coupler with wideband quadrature phase balance, Microw. Opt. Technol. Lett. 58 (6) (2016) 1369–1374, https://doi.org/10.1002/mop.29798.
[20] F.H. Ahmed, R. Saad, S.K. Khamas, A novel compact broadband quasi-twisted branch line coupler based on a double-layered microstrip line, Micromachines 15 (2024) 142.
[21] N.A.M. Shukor, N. Seman, 5G planar branch line coupler design based on the analysis of dielectric constant, loss tangent and quality factor at high frequency, Nature scientific reports 10 (2020) 16115, https://doi.org/10.1038/s41598-020-72444-2.
[22] A. Rezaei, L. Noori, A microstrip hybrid coupler with a wide stop-band using symmetric structure for wireless applications, Journal of Microwaves, Optoelectronics and Electromagnetic Applications 17 (1) (2018) 23–31, https://doi.org/10.1590/2179-10742018v17i11121.
[23] A.A. Abdulbari, S.K.A. Rahim, M.Z.A.A. Aziz, K.G. Tan, N.K. Noordin, M.Z.M. Nor, New design of wideband microstrip branch line coupler using T-shape and open stub for 5G application, Int. J. Electr. Comput. Eng. 11 (2) (2021) 1346–1355, https://doi.org/10.11591/ijece.v11i2.pp1346-1355.
[24] J. Shi, J. Qiang, K. Xu, Z.b. Wang, L. Lin, J.X. Chen, W. Liu, X.Y. Zhang, A balanced filtering branch-line coupler, IEEE Microw. Wireless Compon. Lett. 26 (2) (2016) 119–121, https://doi.org/10.1109/LMWC.2016.2516764.
[25] N.A.M. Shukor, N. Seman, Enhanced design of two-section microstrip-slot branch line coupler with the overlapped k/4 open circuited lines at ports, Springer Wireless Personal Communications 88 (3) (2016) 467–478, https://doi.org/10.1007/s11277-015-3138-z.
[26] C.Y. Liou, M.S. Wu, J.C. Yeh, Y.Z. Chueh, S.G. Mao, A novel triple-band microstrip branch-line coupler with arbitrary operating frequencies, IEEE Microw. Wireless Compon. Lett. 19 (11) (2009) 683–685, https://doi.org/10.1109/LMWC.2009.2031998.
[27] U. Patel, T. Upadhyaya, V. Sorathiya, K. Pandya, A. Alwabli, K. Dave, N.F. Soliman, W. El-Shafai, Split ring resonator geometry inspired crossed flower shaped fractal antenna for satellite and 5G communication applications, Results in Engineering 22 (2024) 102110.
[28] A. Rezaei, S.I. Yahya, L. Nouri, A high-performance microstrip bandpass filtering coupler with low-loss and compact size, Microw. Opt. Technol. Lett. 65 (9) (2023) 2483–2487, https://doi.org/10.1002/mop.33732.
[29] J.K. Xiao, R.N. Shi, C.F. Huang, Filtering couplers based on multi-layer self-packaged suspended coplanar waveguide hybrid and coupled techniques, AEU-International Journal of Electronics and Communications 174 (2024) 155022, https://doi.org/10.1016/j.aeue.2023.155022.
[30] J.S. Hong, M.J. Lancaster, Microstrip Filters for RF/Microwave Applications, John Wiley & Sons, 2001, https://doi.org/10.1002/0471221619.
[31] J. Xu, Z.Y. Chen, H. Wan, Lowpass-bandpass triplexer integrated switch design using common lumped-element triple-resonance resonator technique, IEEE Trans. Ind. Electron. 67 (1) (2020) 471–479, https://doi.org/10.1109/TIE.2019.2898579.
[32] M. Hayati, A.R. Zarghami, S. Zarghami, S. Alirezaee, Designing a miniaturized microstrip lowpass-bandpass diplexer with wide stopband by examining the effects between filters, AEU-International Journal of Electronics and Communications 139 (2021) 153912, https://doi.org/10.1016/j.aeue.2021.153912.
[33] Y. Liu, A tri-band bandpass filter realized using tri-mode T-shape branches, Prog. Electromagn. Res. 105 (2010) 425–444, https://doi.org/10.2528/PIER10010902.
[34] F.C. Chen, J.M. Qiu, H.T. Hu, Q.X. Chu, M.J. Lancaster, Design of microstrip lowpass bandpass triplexer with high isolation, IEEE Microw. Wireless Compon. Lett. 25 (12) (2015) 805–807, https://doi.org/10.1109/LMWC.2015.2496797.
[35] S.C. Lin, Microstrip dual/quad-band filters with coupled lines and quasi-lumped impedance inverters based on parallel-path transmission, IEEE Trans. Microw. Theor. Tech. 59 (8) (2011) 1937–1946, https://doi.org/10.1109/TMTT.2011.2142191.
[36] K.A. Majdi, Y.S. Mezaal, New miniature narrow band microstrip diplexer for recent wireless communications, Electronics 12 (3) (2023) 716, https://doi.org/10.3390/electronics12030716.

[37] M. Danaeian, Miniaturized half-mode substrate integrated waveguide diplexer based on SIR–CSRR unit-cell, Analog Integr. Circuits Signal Process. 102 (2020) 555–561, https://doi.org/10.1007/s10470-019-01528-5.
[38] M. Hayati, M. Ekhteraei, F. Shama, A compact microstrip lowpass filter with flat group-delay and ultra high figure-of-merit, Appl. Comput. Electromagn. Soc. J. 32 (2) (2017) 147–152. https://journals.riverpublishers.com/index.php/ACES/article/view/9739/8139.
[39] E.A. Meseldzija, J. Anastasov, D.N. Milic, A linear group delay filter with tunable positive slope for analog signal processing, Int. J. Circ. Theor. Appl. 49 (5) (2021) 1307–1326, https://doi.org/10.1002/cta.2995.